Title	Equiaxed grain formation by intrinsic heterogeneous nucleation via rapid heating and cooling in additive manufacturing of aluminum-silicon hypoeutectic alloy
Author(s)	Okugawa, Masayuki; Ohigashi, Yuta; Furishiro, Yuya et al.
Citation	Journal of Alloys and Compounds. 2022, 919, p. 165812
Version Type	VoR
URL	https://hdl.handle.net/11094/89745
rights	This article is licensed under a Creative Commons Attribution 4.0 International License.
Note	

Equiaxed grain formation by intrinsic heterogeneous nucleation via rapid heating and cooling in additive manufacturing of aluminum-silicon hypoeutectic alloy

Masayuki Okugawa [a,b], Yuta Ohigashi [a], Yuya Furishiro [a], Yuichiro Koizumi [a,b,*], Takayoshi Nakano [a,b]

[a] Division of Materials and Manufacturing Science, Graduate School of Engineering, Osaka University, 2-1 Yamadaoka, Suita, Osaka 565-0871, Japan
[b] Anisotropic Design & Additive Manufacturing Research Center, Osaka University, 2-1 Yamadaoka, Suita, Osaka 565-0871, Japan

ARTICLE INFO

ABSTRACT

The high strength of Al-Si hypoeutectic alloys additively manufactured by powder-bed fusion is of great scientific interest. To date, the mechanism of grain refinement near the fusion line, which contradicts conventional Hunt's columnar–equiaxed transition criteria, remains to be elucidated. Here we present the first report on the mechanism of grain refinement. When a laser was irradiated on cast Al-Si alloy consisting of coarse α-Al grain and α-Al/Si eutectic regions, grain refinement occurred only near the eutectic regions. This strongly suggests that the Si phase is crucial for grain refinement. Multi-phase-field simulation revealed that rapid heating due to the laser irradiation results in unmelted Si particles even above the liquidus temperature and that the particles act as heterogeneous nucleation sites during the subsequent re-solidification. These results suggest the feasibility of a novel inoculant-free grain refinement that is applicable to eutectic alloys comprising phases with a significant melting point difference.

1. Introduction

Additively manufactured (AMed) aluminum (Al) alloy parts are being increasingly employed in industrial applications, in particular transport equipment, such as automobiles, motorcycles, airplanes, and spaceplanes, because of their high specific strength, high fatigue resistance, and the degree of freedom in their shape [1–14]. Al alloys with an equiaxed microstructure show good mechanical properties. Therefore, commonly used AMed Al alloys also have fine equiaxed grains, which are achieved by introducing rare-earth inoculant elements to form dissoluble particles as heterogeneous nucleation sites [1–5]. However, expensive rare-earth inoculant elements substantially increase the cost of the powder. Therefore, a novel grain-refining additive manufacturing (AM) process is required.

We focus on an anomalous microstructure of aluminum-silicon (Al-Si) hypoeutectic alloy fabricated by laser powder bed fusion (L-PBF)-type AM as a potential clue for developing such a process. In general, solidification microstructures are predicted by Hunt's columnar–equiaxed transition (CET) criteria [15–22]. According to Hunt's CET criteria, solidification conditions are defined by the combination of the temperature gradient (G) at a solid–liquid interface and the migration velocity of the interface (R): Columnar dendrites are expected to be formed near a melt pool boundary under high-G and low-R conditions, whereas equiaxed grains are expected to form at the center of a melt pool under low-G and high-R conditions. In fact, such microstructures are commonly observed in L-PBFed Ni alloys [23]. However, the relations between microstructures and solidification conditions for Al-Si hypoeutectic alloys show an opposing trend to those predicted by the CET criteria [7,9,11]: equiaxed grains appear near the boundary of a melt pool (i.e., the fusion line), and columnar dendrites are observed in the center of the melt pool (Fig. 1). Note that the equiaxed grains seem to be similar to that observed in a chill zone which appear near a cold mold wall in a casting process due to a high cooling rate [24]. However, at the melt pool boundary in the L-PBF process, the cooling rate which can be represented by $R \times G$ is zero because the R is zero at the melt pool boundary where is the turning point of melting and solidification. Therefore, the equiaxed crystalline grains cannot be explained by the same mechanism as that for a chill zone.

* Corresponding author at: Division of Materials and Manufacturing Science, Graduate School of Engineering, Osaka University, 2-1 Yamadaoka, Suita, Osaka 565-0871, Japan.
*E-mail address:* ykoizumi@mat.eng.osaka-u.ac.jp (Y. Koizumi).
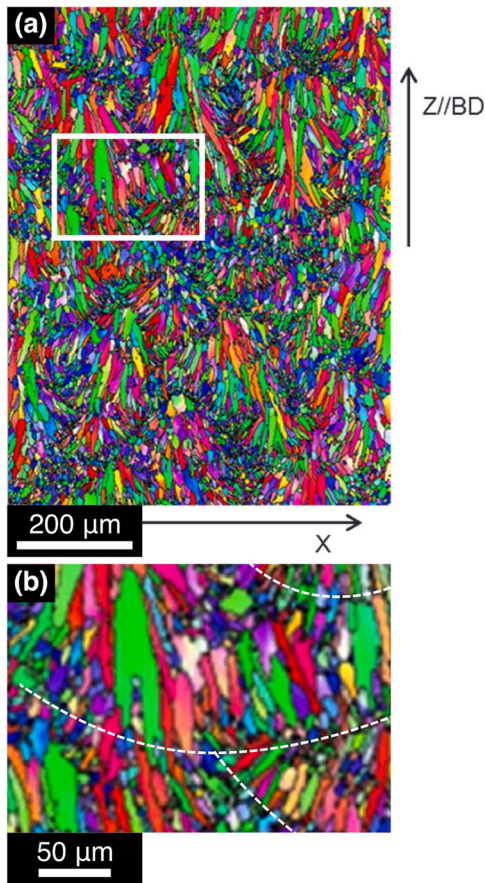
Fig. 1. SEM-EBSD inverse-pole-figure (IPF) orientation maps of AMed AlSi10Mg. (b) Magnified view of the framed region in the rectangle in (a). White dashed lines indicate fusion lines.
Adapted from Ref. [1], Copyright (2017), with permission from Elsevier.

Fig. 2. (a) SEM secondary-electron image of as-cast Al-Si hypoeutectic sample. (b) SEM back-scattering electron image of cross section of the laser-irradiated region and (c), (d) corresponding EDS element map ((c) Al, (d) Si) and (e) EBSD IPF orientation map.

A similar anomalous microstructure was observed in inoculated AMed Al alloys [1–5]; specifically, inoculant compounds with high melting points remain undissolved near the fusion line in the heating process and act as heterogeneous nucleation sites for equiaxed grains. The similarities in the microstructure suggest that the unique equiaxed grains observed in Al-Si hypoeutectic alloys can also be formed by a heterogeneous nucleation mechanism. In the powder bed fusion (PBF)–type additive manufacturing process, melting and solidification respectively occur at high heating and cooling rates up to around 10^6 K s^{-1} [25]. Regions near the fusion line (i.e., the isotemperature line for the liquidus of the alloy) are heated to a temperature slightly above the liquidus temperature and melted only for several tens of microseconds [26]. We suggest that crystalline Si particles remain unmelted even after the re-melting process (i.e., formation of a melt pool) and act as heterogeneous nucleation sites for equiaxed grains in the re-solidification process owing to the large difference of approximately 750 K between the melting points of Al (933 K) and Si (1687 K) [27] and the exceptionally short time span of the rapid melting process, which allows the only limited dissolution of Si particles. However, this scenario is still to be justified by both experiment and modelling.

In this study, we demonstrate for the first time the successful use of the aforementioned grain refinement mechanism based on a combination of a laser irradiation experiment on a bulk Al-10 mass% Si hypoeutectic alloy and corresponding multiphase-field simulation (MPF) of melting by rapid heating followed by solidification via rapid cooling.
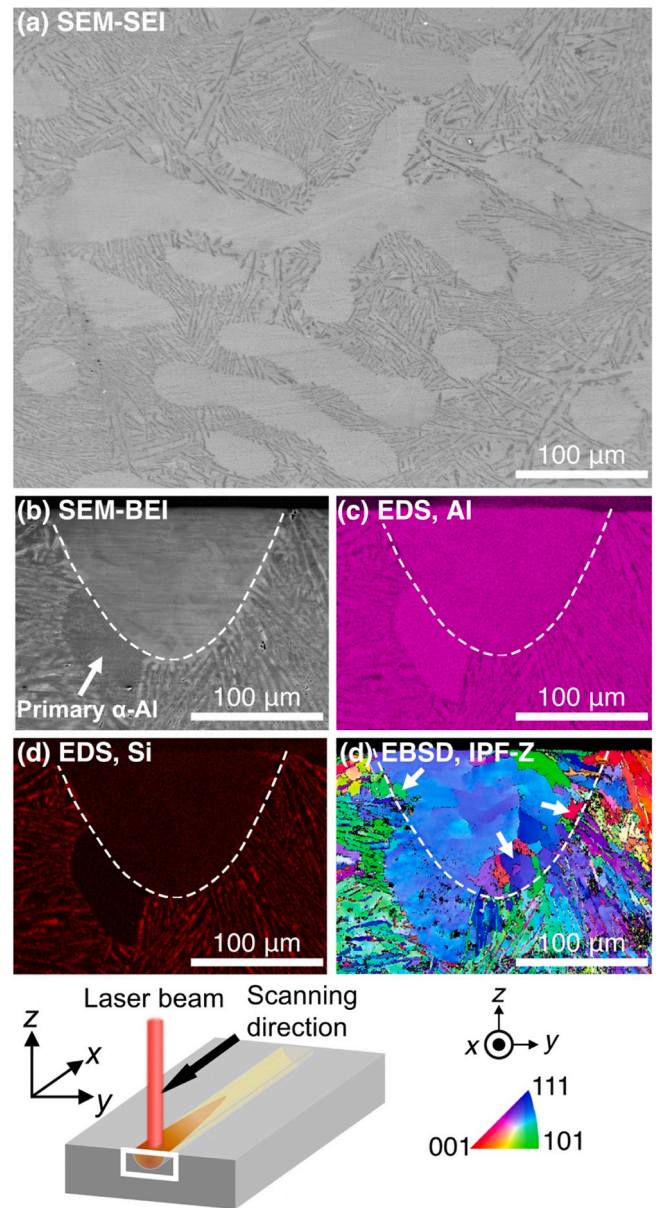
2. Method

2.1. Experimental procedure

The laser-beam irradiation experiment was performed as follows. Ingots of Al-10 mass% Si were prepared by melting Al with 99.99 mass% purity and Si with 99.999 mass% purity in alumina crucibles at 973 K in an argon atmosphere. Fig. 2(a) shows a secondary electron image of the as-cast microstructure of the Al-Si alloy observed by a field-emission scanning electron microscope (FE-SEM, JEOL JIB-4610 F). The microstructure consists of primary α-Al crystals with a diameter of approximately 50 μm and eutectic colonies with an average lamellar spacing of approximately 5 μm. A region including both a primary α-Al and an eutectic domain was irradiated with a scanning laser beam using a L-PBF machine (EOS M290). The laser power and scanning speed were 360 W and 1000 mm s^{-1}, respectively. The crystal orientations and chemical compositions were

analyzed using electron-backscattering diffraction (EBSD) and an energy-dispersive X-ray spectrometer (EDS).

2.2. Computational method

Two-dimensional MPF simulations of a simplified Al-10 mass% Si model were performed to reveal the microstructure formation process in the regions near the eutectic colonies using the Microstructure Evolution Simulation Software (MICRESS) [28,29] with TQ-Interface for Thermo-Calc [30]. The Gibbs free energy and diffusion potential of the Al-Si binary system were calculated using CALPHAD data [31]. The simulation domain size was 50 μm × 100 μm. The grid size Δx and interface width were set to be 1 μm and 3.5 μm, respectively. Heterogeneous nucleation was assumed for solid Si-phase (with diamond structure) from the α-Al solid/liquid interface and for α-Al solids from the solid Si-phase/liquid interface. In accordance with reports of MPF simulations for solidification of Al-Si alloys by Eiken et al. [32,33], the interface energies corresponding to α-Al/liquid, Si/liquid, α-Al/α-Al, and α-Al/Si were set as 165, 352, 150, and 380 mJ m^{-2}, respectively. For the interface mobility, a value of 5.0×10^{-10} m^4 J^{-1} s^{-1} was used. As an initial condition, five crystalline Al nuclei with random orientations were placed at the bottom of the simulation domain, and the remaining portion was set as Al-10 mass% Si liquid. The temperature at the bottom was initially set at 865 K, i.e., 20 K below the liquidus temperature. Solidification was simulated under the condition of a cooling rate of 10^4 K s^{-1}, a temperature gradient (G) of 10^6 K m^{-1}, and an interface velocity (R) of 10^{-2} m s^{-1}. Then, the solidified model was re-melted at a heating rate of 10^4 K s^{-1}. After melting up to 75 μm of the material from the upper edge, i.e., 75% (3/4) of the simulation domain, the re-melted model was re-solidified at a cooling rate of 10^4 K s^{-1}, which is the same as the rate of initial solidification.

3. Results and discussion

Fig. 2(**b–e**) show the SEM cross-sectional backscattering electron image (BEI) and corresponding EDS elemental and EBSD orientation maps of the laser-beam-irradiated region in the Al-Si alloy ingot. There are α-Al and eutectic regions outside the fusion line, indicated by the white dashed line in Fig. 2(**b**). The corresponding EDS elemental maps, shown in Fig. 2(**c**) and (**d**), exhibit no contrast in the melt-pool region. This result suggests that solute elements are homogeneously distributed during laser melting, at least on a micrometer scale, because of high atomic diffusivity in the liquid phase and high fluid flow. As shown in Fig. 2(**e**), microstructures that appeared in the melted region depended on the microstructures of the exterior regions. Equiaxed grains were observed near the eutectic microstructure regions, as indicated by the arrows in Fig. 2(**e**). This microstructure is essentially the same as the previously reported microstructures in L-PBFed Al-Si-based alloys [7,9,11]. By contrast, no equiaxed grain was formed near the large primary α-Al grain, and epitaxial growth occurred. As shown in the EDS elemental maps (Fig. 2(**c**) and 2(**d**)), the re-solidified melt-region has homogeneous solute concentration distributions. This suggests that the fluids formed by melting mixed completely before re-solidification on a micrometer scale. This result indicates that the same Al-10 mass% Si alloy liquid re-solidified in the regions near the large primary α-Al grain and near the eutectic microstructure. It should be noted that the shape of the melt-region is symmetric with respect to the vertical center of the image. However, the microstructures outside of the melt-region is asymmetric as seen in Fig. 2(b). A large primary α-Al grain exist to the lower left of the melt region, whereas a eutectic structure is in the corresponding location on the righthand-side. There is no fine grain in the left area near the fusion line facing the large α-grain on the left while fine grains were frequently observed in the corresponding area on the right-hand side. This suggests the

probability of nucleation were different in the left region and the right region. Moreover, the two regions are suggested to be re-solidified under almost the same condition because solidification conditions are determined by a distance from a melt pool boundary in the PBF type AM process. Therefore, the equiaxed grains should appear in both regions if the nucleation is caused by the homogeneous nucleation mechanism. However, in the actual microstructure, equiaxed grains were observed only in the areas near the eutectic microstructural regions.

Fig. 3 shows MPF models of solidified (Fig. 3(**a1**) and (**b1**)), re-melted (Fig. 3(**a2**) and (**b2**)), and re-solidified (Fig. 3(**a3**) and (**b3**)) Al-Si eutectic alloy colored based on Si concentration (Fig. 3(**a1–a4**)) and crystal-orientation angle (Fig. 3(**b1–b4**)). The solidification condition defined by $G = 10^6$ K m^{-1} and $R = 10^{-2}$ m s^{-1} was employed. In the simulated solidification microstructure, as shown in Fig. 3(**a1**) and (**b1**), columnar α-Al crystals with a width of approximately 5 μm appeared elongated along the temperature gradient direction. Eutectic regions comprising α-Al and Si phases formed between dendritic columnar crystals and between secondary arms. The solidified Al-Si alloy model was heated until the melting of 75 μm from the upper edge, as shown in Fig. 3(**a2**) and (**b2**). The white dashed line in Fig. 3(**a2**) indicates the fusion line (defined as the isotemperature line) for the liquidus of the Al-10 mass% Si alloy. The solidified microstructure melted inhomogeneously: columnar dendrites of the α-Al phase were fully melted, whereas the regions with the eutectic microstructure were melted partially and the crystalline solid Si-phase particles remained, as indicated by the arrows in Fig. 3(**a2**). The re-melted Al-Si eutectic alloy model cooled again and re-solidified, as shown in Fig. 3(**a3**) and (**b3**). Dendrites grew isotropically near the fusion line, and equiaxed grains ~20 μm in diameter were formed. The center positions of the equiaxed grains are the same as those of the remaining Si particles observed in the re-melted model in Fig. 3(**a2**) and (**b2**). This indicates that the remaining Si particles act as heterogeneous nucleation sites during the re-solidification process under high heating and cooling rates such as those in the L-PBF process. Notably, not all of the remaining Si crystalline particles observed in the re-melted model become heterogeneous nucleation sites in the re-solidification process. To investigate the microstructure formed in front of the equiaxed grains, the MPF simulation of continued solidification subsequent to the re-solidified state (Fig. 3(**a3**) and (**b3**)) was performed using moving-frame boundary conditions. Fig. 3(**a4**) and (**b4**) show the Si concentration map and the crystal orientation map of the re-solidified MPF model, respectively. Equiaxed grains formed near the fusion line, whereas columnar crystals appeared in the upper region. This simulated microstructure is quite similar to those observed in AlSi10Mg parts built by L-PBF [7,9,11], as shown in Fig. 1. These results suggest that the experimentally observed equiaxed grains were formed by heterogeneous nucleation at the remaining small solid Si phases.

Fig. 4 shows schematics of the evolution of the microstructures during the re-melting and re-solidification processes at low and high heating rates. Let us assume that the initial microstructure consists of α-Al and eutectic phases, as illustrated in Fig. 4(**a**). Under a low-heating-rate condition, the eutectic phase of the Al-Si hypoeutectic alloy melts initially at the eutectic temperature, as illustrated in Fig. 4(**b1**). Then, the α-Al primary crystals melt at the liquidus temperature, as shown in Fig. 4(**b2**). By contrast, under a rapid-heating condition such as that encountered in PBF-type additive manufacturing processes, only a short period of several tens of microseconds is allowed for atomic diffusion between the α-Al and solid Si-phases in eutectic regions. Consequently, the crystalline Si particles remain as illustrated in Fig. 4(**c2**). When re-solidification initiates from the inhomogeneous liquid (Fig. 4(**c2**)), some of the Si crystalline particles act as heterogeneous nuclei for the formation of α-Al equiaxed grains (Fig. 4(**c3**)). To obtain direct evidence for this prediction, three-dimensional observation experiment by serial
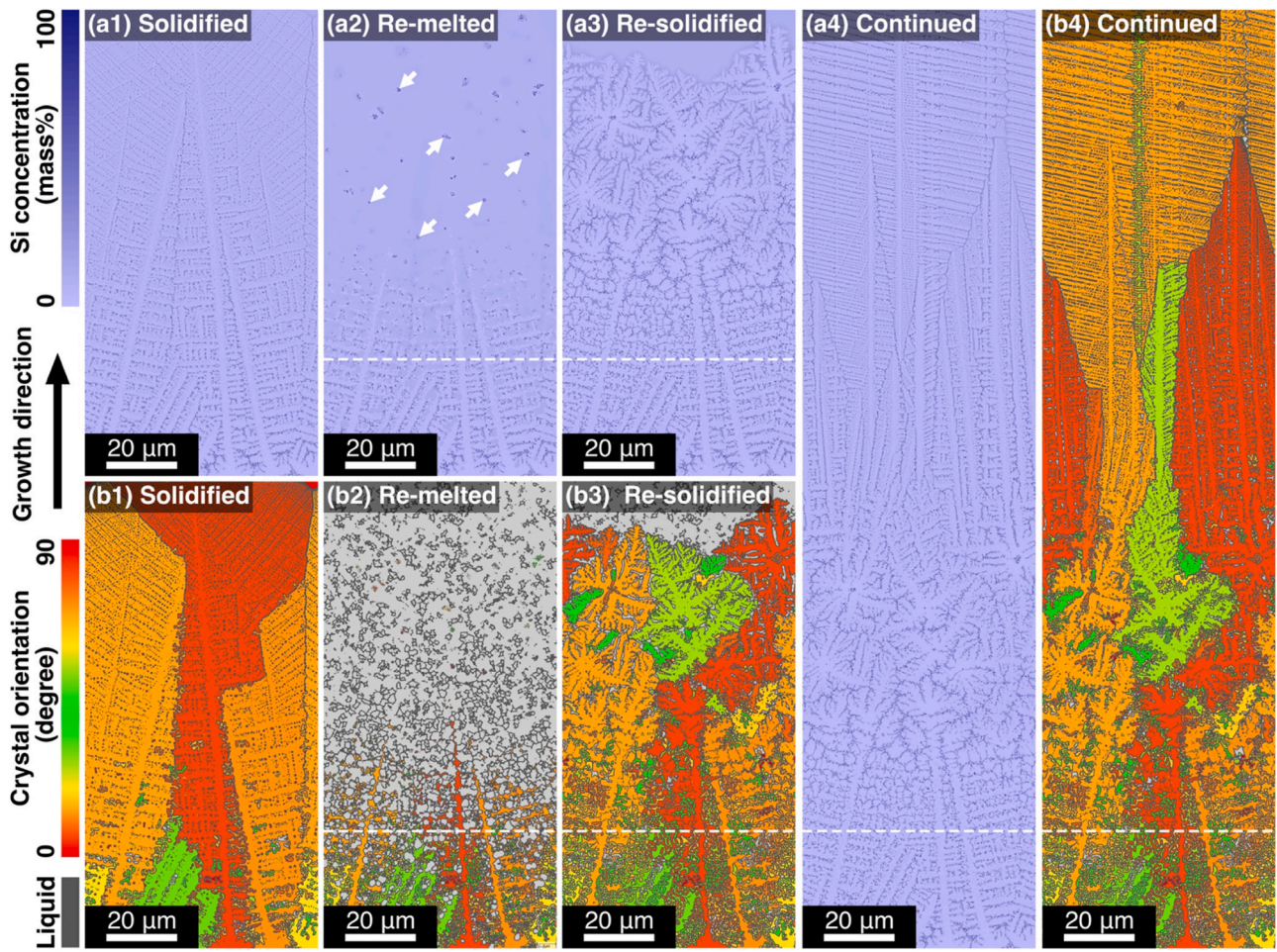
Fig. 3. (a1–a4) Concentration maps and (b1–b4) crystal orientation maps of microstructures generated by MPF simulations of the sequential rapid solidification/re-melting/re-solidification process: (a1, b1) Solidified, (a2, b2) re-melted, (a3, b3) re-solidified, and (a4, b4) after continued solidification subsequent to the re-solidified state simulated using the moving-frame boundary condition.
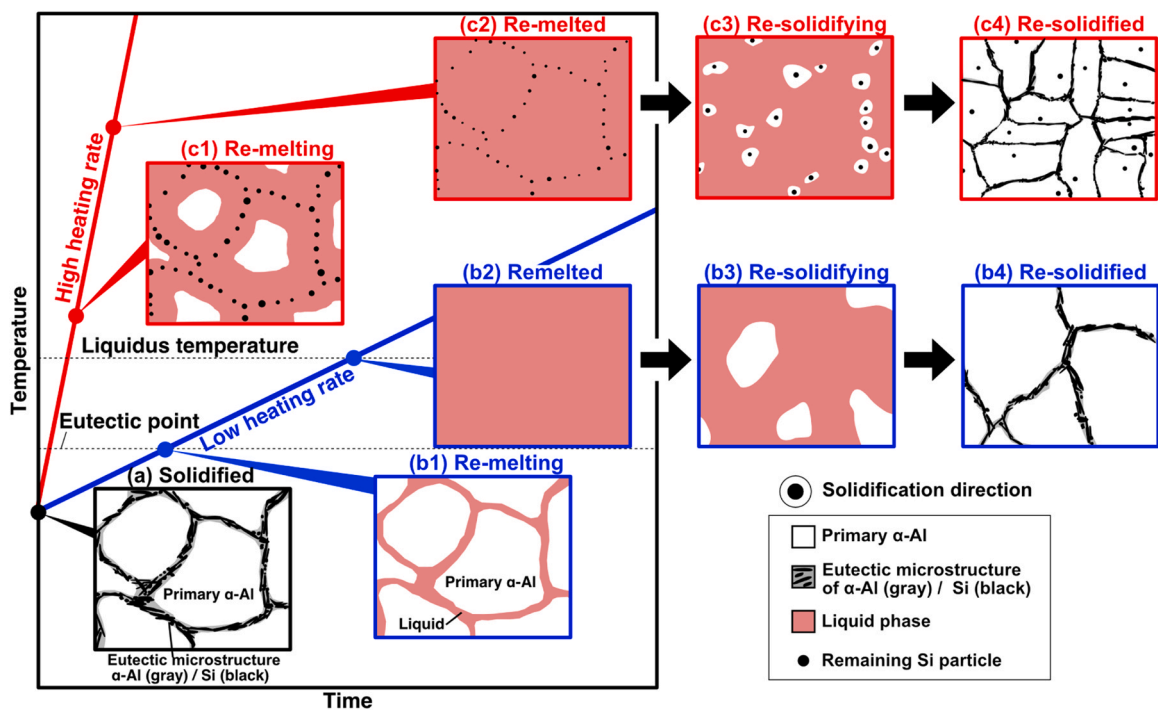

Fig. 4. Schematic illustrations of re-melting and re-solidification behavior under (b1–b4) low- and (c1–c4) high-heating-rate conditions.

sectioning methods of ʟ-PBFed Al-Si samples and an in-situ TEM observation experiment of melt and solidification of Al-Si thin films under rapid heating and cooling conditions are currently underway.

4. Conclusion

In summary, we demonstrated that equiaxed grains near the fusion line in a ʟ-PBF-built Al-Si alloy are formed by an intrinsic heterogeneous nucleation mechanism. We performed a laser-irradiation experiment and microstructure analysis on an as-cast Al-Si alloy ingot consisting of coarse α-Al grains and α-Al/Si eutectic regions. Notably, grain refinements occurred only near the eutectic region containing a solid Si phase. MPF simulations revealed that Si crystalline particles remain near the fusion line even after the rapid re-melting process, serving as heterogeneous nucleation sites in the re-solidification process. The crystalline Si particles remain owing to the substantial melting point difference of approximately 750 K between α-Al and solid Si phases and the short diffusion time during the rapid re-melting process. Our study revealed that grain refinement can occur by an intrinsic heterogeneous nucleation mechanism in an Al-Si alloy. This effect can be used to achieve a novel inoculant-free fine-graining process. Moreover, the technique could possibly be applied to other eutectic alloys with a large difference in the melting points of constituent phases.

CRediT authorship contribution statement

Masayuki Okugawa: Conceptualization, Methodology, Writing – review & editing, Computer simulation, Data curation, Visualization. **Yuta Ohigashi**: Computer simulation, Data curation. **Yuya Furishiro**: Computer simulation, Data curation, Visualization. **Yuichiro Koizumi**: Conceptualization, Supervision, Editing. **Takayoshi Nakano**: Supervision.

Declaration of Competing Interest

The authors declare the following financial interests/personal relationships which may be considered as potential competing interests: Masayuki Okugawa reports financial support was provided by the Japan Aluminium Association. Masayuki Okugawa reports financial support was provided by Japan Society for the Promotion of Science. Yuichiro Koizumi reports financial support was provided by Japan Society for the Promotion of Science.

Acknowledgements

References

[1] H. Zhang, H. Zhu, X. Nie, J. Yin, Z. Hu, X. Zeng, Effect of zirconium addition on crack, microstructure and mechanical behavior of selective laser melted Al-Cu-Mg alloy, Scr. Mater. 134 (2017) 6–10, https://doi.org/10.1016/j.scriptamat.2017.02.036

[2] J.H. Martin, B.D. Yahata, J.M. Hundley, J.A. Mayer, T.A. Schaedler, T.M. Pollock, 3D printing of high-strength aluminium alloys, Nature 549 (2017) 365–369, https://doi.org/10.1038/nature23894

[3] K.V. Yang, Y. Shi, F. Palm, X. Wu, P. Rometsch, Columnar to equiaxed transition in Al-Mg(-Sc)-Zr alloys produced by selective laser melting, Scr. Mater. 145 (2018) 113–117, https://doi.org/10.1016/j.scriptamat.2017.10.021

[4] A. Aversa, G. Marchese, A. Saboori, E. Bassini, D. Manfredi, S. Biamino, D. Ugues, P. Fino, M. Lombardi, New aluminum alloys specifically designed for laser powder bed fusion: a review, Mater. (Basel). 12 (2019) 1007, https://doi.org/10.3390/ma12071007

[5] M. Yi, P. Zhang, C. Yang, P. Cheng, S. Guo, G. Liu, J. Sun, Improving creep resistance of Al-12 wt% Ce alloy by microalloying with Sc, Scr. Mater. 198 (2021) 113838, https://doi.org/10.1016/j.scriptamat.2021.113838

[6] M. Tang, P.C. Pistorius, S. Narra, J.L. Beuth, Rapid solidification: selective laser melting of AlSi10Mg, Jom 68 (2016) 960–966, https://doi.org/10.1007/s11837-015-1763-3

[7] J. Liu, W. Xiong, A. Behera, S. Thompson, A.C. To, Mean-field polycrystal plasticity modeling with grain size and shape effects for laser additive manufactured FCC metals, Int. J. Solids Struct. 112 (2017) 35–42, https://doi.org/10.1016/j.ijsolstr.2017.02.024

[8] Y. Yang, Y. Chen, J. Zhang, X. Gu, P. Qin, N. Dai, X. Li, J.-P. Kruth, L.-C. Zhang, Improved corrosion behavior of ultrafine-grained eutectic Al-12Si alloy produced by selective laser melting, Mater. Des. 146 (2018) 239–248, https://doi.org/10.1016/j.matdes.2018.03.025

[9] N. Takata, H. Kodaira, A. Suzuki, M. Kobashi, Size dependence of microstructure of AlSi10Mg alloy fabricated by selective laser melting, Mater. Charact. 143 (2018) 18–26, https://doi.org/10.1016/j.matchar.2017.11.052

[10] N.T. Aboulkhair, M. Simonelli, L. Parry, I. Ashcroft, C. Tuck, R. Hague, 3D printing of aluminium alloys: additive manufacturing of aluminium alloys using selective laser melting, Prog. Mater. Sci. 106 (2019) 100578, https://doi.org/10.1016/j.pmatsci.2019.100578

[11] X. Liu, C. Zhao, X. Zhou, Z. Shen, W. Liu, Microstructure of selective laser melted AlSi10Mg alloy, Mater. Des. 168 (2019) 107677, https://doi.org/10.1016/j.matdes.2019.107677

[12] I.M. Kusoglu, B. Gökce, S. Barcikowski, Research trends in laser powder bed fusion of Al alloys within the last decade, Addit. Manuf. 36 (2020) 101489, https://doi.org/10.1016/j.addma.2020.101489

[13] H. Bian, K. Aoyagi, Y. Zhao, C. Maeda, T. Mouri, A. Chiba, Microstructure refinement for superior ductility of Al-Si alloy by electron beam melting, Addit. Manuf. 32 (2020) 100982, https://doi.org/10.1016/j.addma.2019.100982

[14] M.N. Patel, D. Qiu, G. Wang, M.A. Gibson, A. Prasad, D.H. StJohn, M.A. Easton, Understanding the refinement of grains in laser surface remelted Al–Cu alloys, Scr. Mater. 178 (2020) 447–451, https://doi.org/10.1016/j.scriptamat.2019.12.020

[15] J.D.D. Hunt, Steady state columnar and equiaxed growth of dendrites and eutectic, Mater. Sci. Eng. 65 (1984) 75–83, https://doi.org/10.1016/0025-5416(84)90201-5

[16] X. Ding, Y. Koizumi, D. Wei, A. Chiba, Effect of process parameters on melt pool geometry and microstructure development for electron beam melting of IN718: a systematic single bead analysis study, Addit. Manuf. 26 (2019) 215–226, https://doi.org/10.1016/j.addma.2018.12.018

[17] S. Bontha, N.W. Klingbeil, P.A. Kobryn, H.L. Fraser, Effects of process variables and size-scale on solidification microstructure in beam-based fabrication of bulky 3D structures, Mater. Sci. Eng. A. 513–514 (2009) 311–318, https://doi.org/10.1016/j.msea.2009.02.019

[18] B. Schoinochoritis, D. Chantzis, K. Salonitis, Simulation of metallic powder bed additive manufacturing processes with the finite element method: a critical review, Proc. Inst. Mech. Eng. Part B J. Eng. Manuf. 231 (2017) 96–117, https://doi.org/10.1177/0954405414567522

[19] J. Gockel, J. Beuth, Understanding Ti-6Al-4V microstructure control in additive manufacturing via process maps, 24th Int. SFF Symp. - An Addit. Manuf. Conf. SFF 2013. (2013) 666–674.

[20] Y. Zhao, Y. Koizumi, K. Aoyagi, D. Wei, K. Yamanaka, A. Chiba, Molten pool behavior and effect of fluid flow on solidification conditions in selective electron beam melting (SEBM) of a biomedical Co-Cr-Mo alloy, Addit. Manuf. 26 (2019) 202–214, https://doi.org/10.1016/j.addma.2018.12.002

[21] A. Prasad, L. Yuan, P. Lee, M. Patel, D. Qiu, M. Easton, D. StJohn, Towards understanding grain nucleation under Additive Manufacturing solidification conditions, Acta Mater. 195 (2020) 392–403, https://doi.org/10.1016/j.actamat.2020.05.012

[22] Y. Miyata, M. Okugawa, Y. Koizumi, T. Nakano, Inverse columnar-equiaxed transition (CET) in 304 and 316L stainless steels melt by electron beam for additive manufacturing (AM), Crystals 11 (2021) 856, https://doi.org/10.3390/cryst11080856

[23] A.S. Sabau, L. Yuan, N. Raghavan, M. Bement, S. Simunovic, J.A. Turner, V.K. Gupta, Fluid dynamics effects on microstructure prediction in single-laser tracks for additive manufacturing of IN625, Metall. Mater. Trans. B. 51 (2020) 1263–1281, https://doi.org/10.1007/s11663-020-01808-w

[24] J. Hutt, D. StJohn, The origins of the equiaxed zone -review of theoretical and experimental work, Int. J. Cast. Met. Res. 11 (1998) 13–22, https://doi.org/10.1080/13640461.1998.11819254

[25] N. Sohrabi, J.E.K. Schawe, J. Jhabvala, J.F. Löffler, R.E. Logé, Critical crystallization properties of an industrial-grade Zr-based metallic glass used in additive manufacturing, Scr. Mater. 199 (2021) 113861, https://doi.org/10.1016/j.scriptamat.2021.113861

[26] A.A. Martin, N.P. Calta, S.A. Khairallah, J. Wang, P.J. Depond, A.Y. Fong, V. Thampy, G.M. Guss, A.M. Kiss, K.H. Stone, C.J. Tassone, J. Nelson Weker, M.F. Toney, T. van Buuren, M.J. Matthews, Dynamics of pore formation during laser powder bed fusion additive manufacturing, Nat. Commun. 10 (2019) 1–10, https://doi.org/10.1038/s41467-019-10009-2

[27] J.L. Murray, A.J. McAlister, The Al-Si (aluminum-silicon) system, Bull. Alloy Phase Diagr. 5 (1984) 74–84, https://doi.org/10.1007/BF02868729

[28] MICRostructure Evolution Simulation Software, phase-field software package, ⟨www.micress.de⟩.

[29] J. Eiken, B. Böttger, I. Steinbach, Multiphase-field approach for multicomponent alloys with extrapolation scheme for numerical application, Phys. Rev. E. 73 (2006) 1–9, https://doi.org/10.1103/PhysRevE.73.066122

[30] J.O. Andersson, T. Helander, L. Höglund, P. Shi, B. Sundman, Thermo-Calc & DICTRA, computational tools for materials science, Calphad 26 (2002) 273–312, https://doi.org/10.1016/S0364-5916(02)00037-8

[31] H. Zhang, Y. Wang, S.L. Shang, C. Ravi, C. Wolverton, L.Q. Chen, Z.K. Liu, Solvus boundaries of (meta)stable phases in the Al-Mg-Si system: First-principles phonon calculations and thermodynamic modeling, Calphad 34 (2010) 20–25, https://doi.org/10.1016/j.calphad.2009.10.009

[32] J. Eiken, M. Apel, S.M. Liang, R. Schmid-Fetzer, Impact of P and Sr on solidification sequence and morphology of hypoeutectic Al-Si alloys: Combined thermodynamic computation and phase-field simulation, Acta Mater. 98 (2015) 152–163, https://doi.org/10.1016/j.actamat.2015.06.056

[33] J. Eiken, M. Apel, Eutectic morphology evolution and Sr-modification in Al-Si based alloys studied by 3D phase-field simulation coupled to Calphad data, IOP Conf. Ser. Mater. Sci. Eng. 84 (2015) 012084, https://doi.org/10.1088/1757-899X/84/1/012084